

THE EFFECTS OF AIR-BORNE WATER MIST ON THE LOCAL BURNING RATE OF A PMMA PLATE IN BOUNDARY LAYER COMBUSTION

C.C. Ndubizu (cmdubizu@castor.nrl.navy.mil 202-767-2766)

Geo-Centers Inc. Lahnam, MD

R Ananth (rananth@castor.nrl.navy.mil 202-767-3197) and F.W Williams

Navy Technology Center for Safety and Survivability

Naval Research Laboratory

Washington D.C 20375

ABSTRACT

This paper presents of an experimental study of the effects of ultra fine water mist ($\sim 3 \mu\text{m}$) and regular spray nozzle mist ($\sim 30 \mu\text{m}$) on forced flow boundary layer combustion of a poly methylmethacrylate plate, where mist was introduced with the incoming air. With the spray nozzles, burning rate downstream was enhanced due to spray-induced turbulence, which enhanced heat feedback rate to the plate in this region. Because of the higher heat feedback rate, the downstream achieves steady state burning rate faster with mist than without mist. On the other hand, the ultra fine mist has no induced turbulence and burning rate was suppressed everywhere along the plate due to mist cooling and dilution effects. Transient burning rate downstream lasts longer in this case due to the lower heat feedback rate.

1.INTRODUCTION

Boundary layer type flames have been widely studied because of their importance in wall fires and wind-aided fires on flat surfaces. Spilled fuel fires on aircraft carrier decks are typical boundary layer type fires, which are of concern to the Navy. Laboratory-scale studies of water mist suppression of fire in a boundary layer combustion configuration are lacking. Tamanini [1] studied the suppression of fire on burning vertical slabs using water mist sprayed horizontally on the fire. He obtained a power-law correlation between the burning rate and the water application rate. Earlier, Magee and Reitz [2] conducted similar experiments, where vertical and horizontal plastic slabs were subjected to turbulent burning with external radiation and horizontal water spray (for the vertical slabs). They determined the critical conditions for extinguishment and showed that for plastics that do not melt excessively the primary mechanism for suppression is by surface cooling. In these large-scale studies water is sprayed perpendicular to the wall fire and the droplets, especially the large ones have a greater chance of reaching the solid surface. In the current study, fine water droplets are mixed with the airflow upstream of a laboratory-scale boundary layer flame and detailed measurements of local temperatures and burning rates are made.

Recently, Ananth et al [3] and also Ndubizu et al [4] have conducted detailed numerical and experimental studies of forced convection boundary layer combustion of PMMA plate without suppressant. They obtained a modified relationship between dimensionless burning rate and Reynolds number Re_x which gives a better prediction of the burning rate at large Re_x and showed that the local burning rate along the plate is transient. In the leading section, the surface regresses

rapidly after ignition leading to the formation of a small valley and a decrease in the heat feedback to the curved surface. As the valley deepens the local burning rate decreases. Downstream the heat feedback from the boundary layer flame to the surface is low and therefore it takes the solid considerable time to warm-up and to pyrolyze at a steady rate. Hence the burning rate increases as the solid warms up. In a similar configuration, Zhuo and Fernandez-Pello [5] studied turbulent burning of a small PMMA plate in forced convection without mist. They showed a linear relationship between local burning rate and $Re_x^{0.5}$ and their results reveal that local burning rate increases significantly with turbulence intensity. Ahmad and Feath [6] conducted a theoretical analysis of a turbulent wall fire without mist. They derived an expression for local burning rate as a function of Raleigh number Ra_x , which fits their experimental data and that of some earlier works fairly well. Their results suggest that transition to turbulence influences burning rate but not very strongly.

This is a continuation of the previous work and it focuses on the effects of water mist on the local burning rate of the PMMA plate. Water mist is injected into the wind tunnel from pressure atomizing nozzles and from an ultrasonic mist generator. Ultrasonic mist generator produces ultra fine mist with droplet diameters of order of $3\ \mu\text{m}$ compared to about 20 to $100\ \mu\text{m}$ for spray droplets. We make detailed temperature measurements in the flame as well as local regression rate measurements and show that there is a significant difference in the way the two systems affect the burning characteristics of the plate.

2. EXPERIMENTAL

Figure 1 shows a schematic of the experimental setup, whose key components include the wind tunnel, the PMMA sample holder and thermocouples mounted on a set of Velmex X-Y unislides. A variable speed blower pumps air into a 36 X 45 X 61 cm plenum at one end of the wind tunnel. Pressure build up in the plenum drives the flow through the wind tunnel and hence the effects of the blower on the flow are minimized. The 30-cm converging section has fine screens and honey comb and connects the plenum to the 15-cm square straight section. Mist is introduced into the airflow after the honeycomb in a small removable chamber. The mixture of air and water mist flows through the remaining 90-cm section of the tunnel to the exit, where the burning PMMA plate is located. The PMMA samples (7.5 x 9.5-cm) are Cyro[®] Acrylite GP plates 2.3 cm thick. The location of the boundary layer flame at the exit instead of inside the tunnel has two advantages. First, we have easy access to move thermocouples in and out of the boundary layer flame to map temperatures. Secondly, we avoid water dripping on the burning surface from the wind tunnel ceiling, which would taint the results.

Solid cone sprays with large droplet ($>10\ \mu\text{m}$) are injected co-currently into the tunnel using Delavan's WDB[®] nozzles by pressure-driving distilled water from a tank through the nozzle. Ultra fine droplets ($\sim 3\ \mu\text{m}$) were produced with an Ultrasonic Mist Generator made by NanoMist Systems LLC. Here, mist is generated outside the tunnel by the ultrasonic vibration of piezoelectric discs under water. Mist is extracted with a small airflow and injected at the floor of the wind tunnel (Fig. 1 Insert). In this paper ultra fine mist will be referred to as NanoMist.

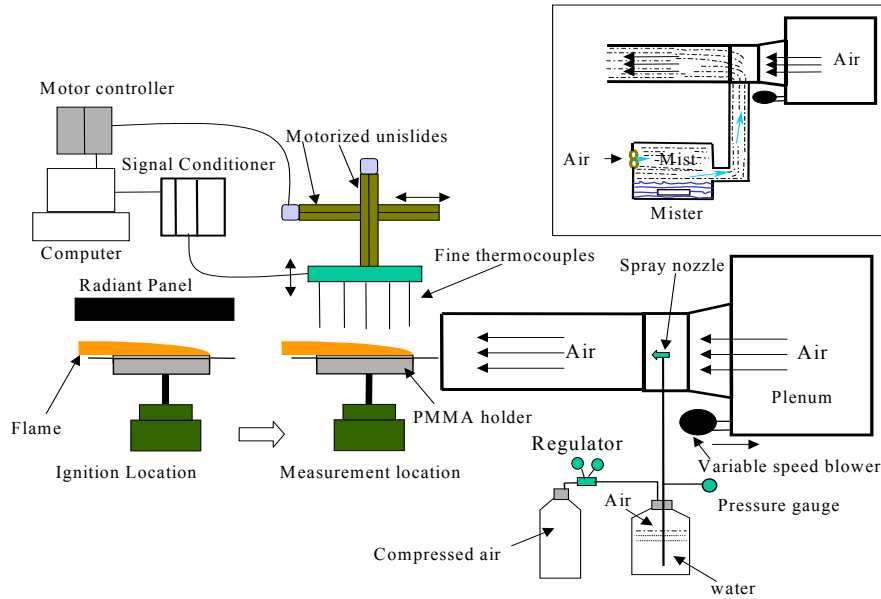


Figure1: Schematic of the test setup with pressure atomizing nozzle and with NanoMist (Insert top right corner)

In tests with mist, the mist and airflow are turned on as the sample surface is uniformly heated and ignited under a radiant panel 40 cm downstream from the tunnel exit (Fig. 1). The process of irradiation, surface gasification and the establishment of a stable 2-D flame over the sample, takes place in about 40 seconds. This gives time for the mist flow to attain steady state. Time is started immediately after ignition. Thereafter, the burning sample is quickly moved to the measurement location at the tunnel exit. Gas phase temperatures are mapped with five R-type thermocouples, 50 μm (0.002”) in diameter, which are mounted on the Velmex[®] X-Y unislides. LabView software is used for motor control as well as continuous temperature data acquisition.

The sample is allowed to burn for a known time interval before the flame is extinguished and the mist flow is turned off. After the sample cools down, its thickness along the centerline is measured at various X locations with a digital micrometer whose accuracy is ± 0.003 mm. Since the initial thickness of the sample was measured, the sample regression rate at each location is obtained as the difference in thickness, after correction for PMMA thermal expansion [4,9] divided by the test duration. Detailed discussion of the thermocouple corrections, temperature errors, expansion corrections and errors in the regression rate were presented in our earlier reports and papers [4,7,8].

2.3 Mist Characterization

The mist parameters were measured dynamically in separate experiments using Malvern Instruments’ Spraytec[®] particle size analyzer. The Malvern Real Time Particle Sizer software is used to obtain droplet size distribution, time-averaged droplet diameters and concentration [7]. The nozzle and mist parameters are given in Table 1. Mist mass loading is the ratio of the “useful” mass flow rate of water and mass flow rate of air. The “useful” mass flow of water is the difference between water injected into the tunnel and what is collected on the tunnel walls

plus what drains out of the tunnel during the test. Mist mass loading was also calculated using the Spraytec[®] concentration data.

Table 2 Nozzle and Mist parameters

Nozzle ID	Orifice diameter (mm)	Pressure (kg/cm ²)	Mist flow rate (cc/min)	Diameter at peak volume frequency (μm)	Peak Volume Frequency (%)	Sauter Mean diameter (μm)	% Mist mass loading (measured)	% Mist mass loading (Spraytec)
SC1	0.33	2.81 (40 psi)	48.8	63	12.9	47.35	1.4	0.44
SC2	0.28	5.27 (75 psi)	42.7	54.86	13.32	39.7	1.0	0.7
SC3	0.28	3.5 (50 psi)	36.1	54.86	12.75	43.14	0.44	0.47
SC4	0.21	70.3 (100 psi)	24.28	36.24	13.82	28.25	1.1	0.49
NanoMist				7.9	7.8	3.16	4.3	1.6

3. RESULTS AND DISCUSSIONS

3.1 Effects of Mist on the Flame Temperature

The spray of mist into the wind tunnel is expected to disturb the airflow despite the co-current arrangement. To investigate the effects of spray-induced instabilities we measured the variation in flame temperature with time at various points in the flame, namely, $Y = 4, 8$ and 12 mm and $X = 22, 37, 57$ and 78 mm, in tests with and without mist. X is the distance from the upstream edge of the plate and Y is the height above the sample surface before ignition. Some of these points are on the fuel side and some are on the airside of the diffusion flame. A typical result for a test with the thermocouple at a downstream location $X=57$ mm, $Y = 8$ mm is shown in Fig. 2. This point is on the airside of the diffusion flame but close to peak temperature location. Figure 2 presents 100 temperature data (20/second) for the base case and four PAN mist cases. Also included for comparison are data from tests with additional nitrogen. As expected the measured temperatures with mist are lower than those without mist due to the cooling effects of mist. Compared to the base case and the nitrogen data the results with Spray nozzles show a much larger scatter, which depicts the effects of flow fluctuations in the flame. For example, while the base case data varied within <50 K, the SC2 data varied within 500 K. Indeed, significantly higher flame fluctuations were observed visually in tests with nozzles.

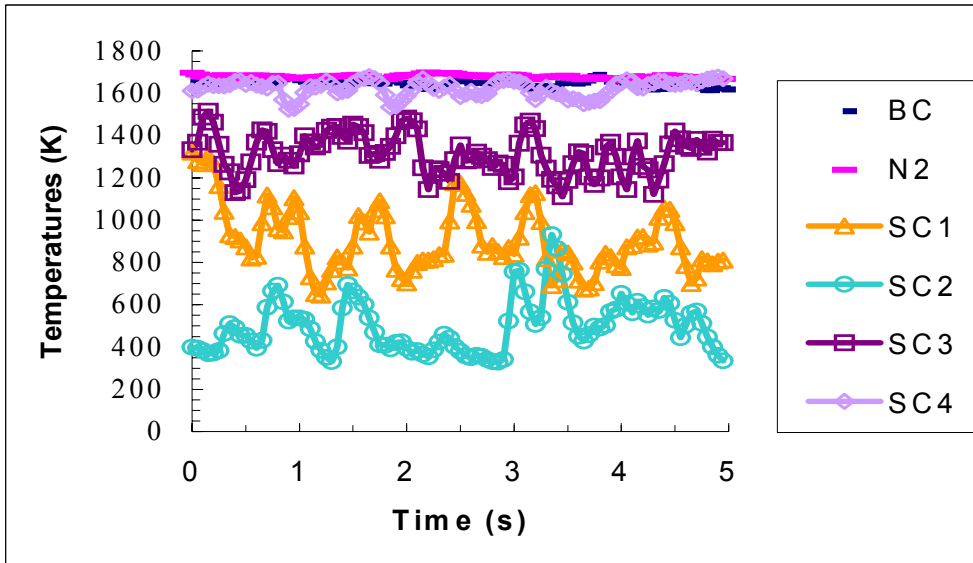
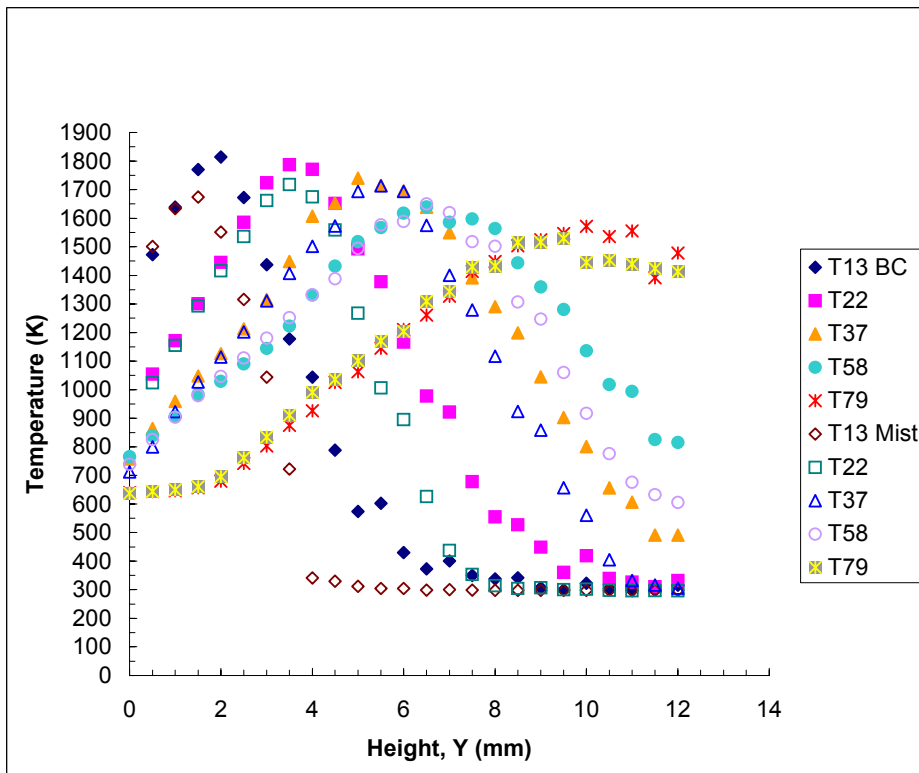


Figure 2: Temperature variation with time at X=57, Y = 8 mm (near the flame front in the trailing section)

The flow disturbance induced by the mist spray action is expected to affect the burning characteristics of the PMMA plate and this will be discussed later.

Figures 3 compare typical temperature profiles at various stream-wise locations in tests with and without (base case) NanoMist and $U_\infty = 84$ cm/s. In Fig.3 the mist mass loading **Figure 3:**



Temperature profiles along the PMMA plate, 13, 22, 37, 58 & 79 mm from upstream edge. Base case and 4.3% NanoMist mass fraction, $U_\infty = 84$ cm/s.

is 4.3%. In the base case tests whose data were compared with NanoMist data we adopted the same airflow arrangement (insert in Fig.1) except that there were no mist droplets. The solid symbols in Fig. 3 represent base case while open symbols represent mist data. The height above the sample refers to the height relative to the PMMA sample surface before the flame was ignited and the surface began to regress. The first and second thermocouples, which were 13 & 22 mm from the leading edge, could not reach the surface of the sample in this location since the surface had regressed a very small distance before the data was taken. Recall that the temperature gradient is very steep in this section and the change in temperature within a gap created by a one-minute regression can be significant as was shown in our earlier work [9]. Therefore, $Y=0$ represents the molten surface more appropriately at large values of X .

Figure 3 shows that NanoMist suppressed flame temperature on the airside of the diffusion flame but not on the fuel side. Suppression in peak temperatures was minimal except near the upstream edge ($X=12$ mm). Temperature suppression is due to the cooling effects of the evaporating droplets and this is more in the leading section than downstream. NanoMist droplets are small with SMD $\sim 3\mu\text{m}$ and therefore the droplets tend to follow the streamlines. Because of their small size their evaporation rate is fast as a result of the d^2 law and hence they probably evaporate before getting to the flame front (peak reaction zone). This explains why the suppression in temperature is only on the airside and hardly on the fuel side and the peak temperatures are not suppressed except near the upstream edge. Further tests were conducted with NanoMist mass loading less than 4.3% but the results show very little suppression in gas phase temperatures. On the other hand because of the rapid cooling in the leading section we could not run more tests with higher mass loading at 84 cm/s without the flame blowing off. The suppression window is very narrow.

Figure 4 shows typical temperature profiles in tests with spray nozzles compared with profiles in the base case test. In this case the mist is from SC3 (Table 1) with SMD $\sim 43\mu\text{m}$ and mist mass loading $\sim 0.44\%$. In the tests with the spray nozzles, a quench zone was formed in the leading section when the flame was moved to the measurement location (Fig. 1). This is due to the rapid cooling from mist. The cooling effects led to an increase in local reaction time and hence a decrease in the local Damkohler number ($Da = \text{flow time}/\text{reaction time}$). Thus the flame retreats and anchors downstream from the leading edge from where it slowly spreads upstream. We had shown in an earlier paper [10], that this unexpected upstream flame-spread is facilitated by the effects of moving boundary. The quench distance in the tests with spray nozzles range from about 2 mm to about 25 mm.

Figure 4 shows that the gas phase temperatures are suppressed on the airside of the diffusion flame at all locations like with NanoMist. However unlike with NanoMist, Fig. 4 shows that the peak temperatures are suppressed at every location along the plate. This suggests that the larger spray droplets probably evaporated closer to the flame front. This would result in more effective use of the latent heat and lead to a rapid reduction in Da in the leading section and make the flame retreat downstream.

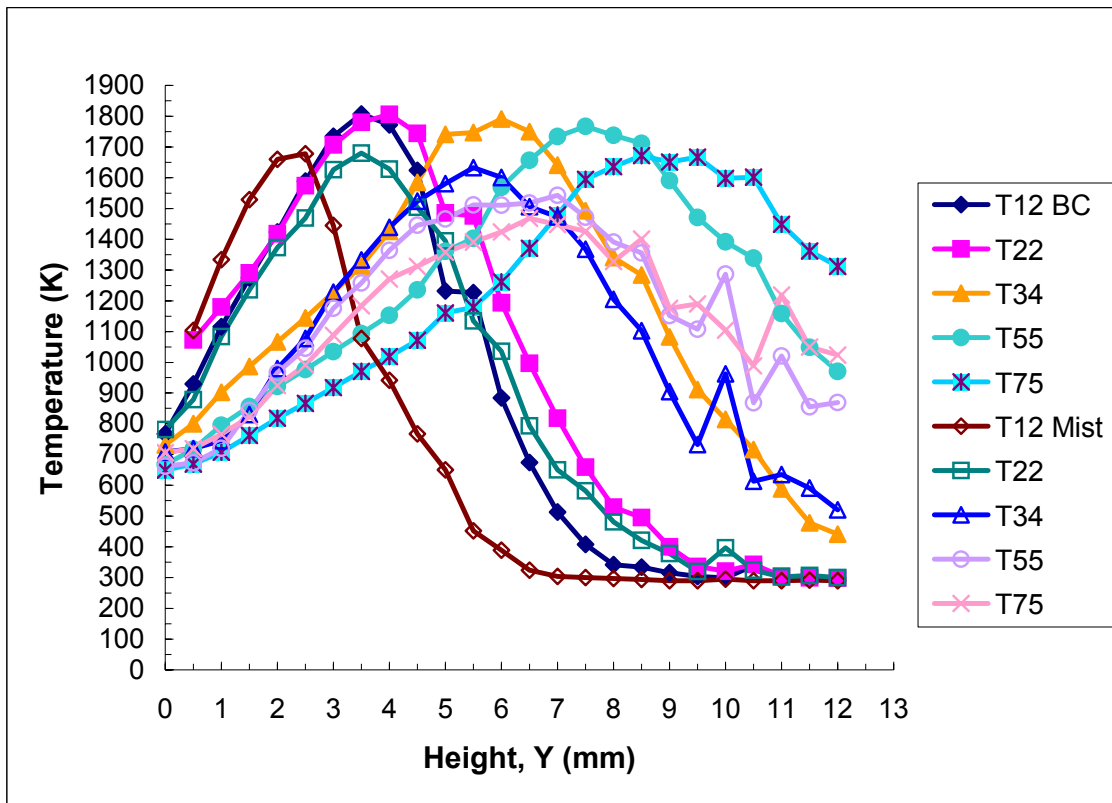


Figure 4: Temperature profiles along the PMMA plate, 12, 22, 34, 55 & 75 mm from upstream edge. Base case and SC3 mist case, $U_{\infty} = 84$ cm/s.

As a result of this, lower mist mass loading would be required to extinguish the flame with spray nozzle mist than with NanoMist. This indeed is the case. For example at $U_{\infty} = 84$ cm/s we require $> 4.3\%$ NanoMist to blow off the flame, while for the same conditions only $> 1.4\%$ SC1 mist is required.

In Fig. 4, since of the flame anchor location shifted downstream (with mist), the thermocouple at $X=12$ mm is closer to the flame leading edge in the mist case than in the base case. Thus the apparent suppression in peak temperature and enhancement in temperature on the fuel side shown at $X= 12$ mm in Fig. 4 are very likely the effects of the flame anchor location rather than the cooling effects of mist. Figure 4 also shows that the flame stand off distance (Y location at peak temperature) δ is smaller in the tests with mist than in the tests without mist. This is more significant for $X > 34$ mm. For example, at $X= 78$ mm, δ is 9 and 6.5 for the base case and mist case, respectively. Also for $X > 34$ mm the gas phase temperature is enhanced on the fuel side of the flame and the temperature gradient on this side seems (qualitatively) to be higher for the mist case than the base case. These effects of mist in the downstream section, namely, smaller δ , higher temperatures and temperature gradients on the fuel side of the flame, strongly suggest that the rate of heat feedback to the PMMA surface is higher in the mist tests than the base case in this section. This would significantly affect the burning rate as we shall show later. Finally Fig. 4 shows a higher temperature fluctuation downstream ($X > 34$ mm) in the tests with mist, especially

on the airside of the flame. This will be shown to correlate with the observed enhancement in heat feedback rate.

3.2 The Effects of Mist on Burning rate

It is well known that the heat feedback to the solid in a boundary layer combustion is very high in the leading section and decreases rapidly with X . We showed in our earlier work [3,4] that the burning rate of the PMMA plate without mist increases with time in the trailing section. This is because it takes the solid considerable time to warm-up and start pyrolyzing at a steady rate because of the slow heat transfer rate and in-depth heat conduction. On the other hand, in the leading section where the heat feedback rate is very high, the surface warms up quickly and regresses rapidly, creating a valley, which deepens with time. As the valley deepens the heat feedback to the curved surface reduces and the regression rate decreases. Next, we present the effects of mist on the PMMA burning characteristics, starting with results in tests with 4.3% NanoMist, which lasted 5, 10 and 20 minutes. The transient effects are seen more clearly in terms of the dimensionless burning rate (Nusselt number) Nu_x , where Nu_x is given [3,4] by

$$Nu_x = R\rho_s LX/(\lambda\Delta T); \quad (1)$$

and R is the local regression rate, ρ_s is the density of air, L is heat of pyrolysis of PMMA (1.6KJ/gm [11]), X is the stream-wise distance from the PMMA leading edge, λ is the thermal conductivity of air and ΔT is the temperature difference between the pyrolyzing surface and the “flame location”. ΔT is estimated as ~ 1200 K since the peak temperature in the flame is ~ 1800 K and molten surface temperature is ~ 600 K [4,9]. Emmons’s steady state equation for the burning rate of PMMA plate obtained from boundary layer analysis is [3,9,12]

$$Nu_x = 0.1 Re_x^{0.5} \quad (2)$$

Figure 5 shows a plot of Nu_x versus $Re_x^{0.5}$, which compares base case with NanoMist results at U_∞ of 84 cm/s. The solid symbols are for the tests without mist while the open symbols are the data with Nanomist. The Emmons’s steady state linear relation is shown as a straight line in Fig. 18. It helps to reveal (qualitatively) the deviation from steady state. At low $Re_x^{0.5}$ (the leading section), the burning rate decreases with time in the tests with and without mist as a result of the moving boundary effects outlined earlier. For example, for $Re_x^{0.5} \sim 16$ ($X \sim 5$ mm), Nu_x is ~ 2.1 , 1.4 and 0.98 for the base case in 5, 10 and 20 minutes, respectively, but it is ~ 1.7 , 0.57, and 0.45 for the mist tests at those times, respectively. Figure 5 shows that the burning rate with NanoMist is less than that without mist at any given time because of cooling.

For large $Re_x^{0.5}$ (the trailing section) the burning rate is significantly less with NanoMist than without mist and in both cases it increases with time. For example, at $Re_x^{0.5} = 70$, the base case Nu_x is ~ 1.75 , ~ 2.75 and ~ 6 in 5, 10 and 20 minute tests, respectively. However, at the same location and times Nu_x is ~ 0.75 , 1.75 and 3, respectively in tests with mist. Again the cooling effects of mist give rise to the lower heat feed back and burning rates. Ananth et al [3,12] reported a steady state numerical solution of Navier Stokes equations for the boundary layer burning of the PMMA plate without mist. Their results compare well with experimental data at long times and both reveal that steady state is attained later as Re_x (X) increases.

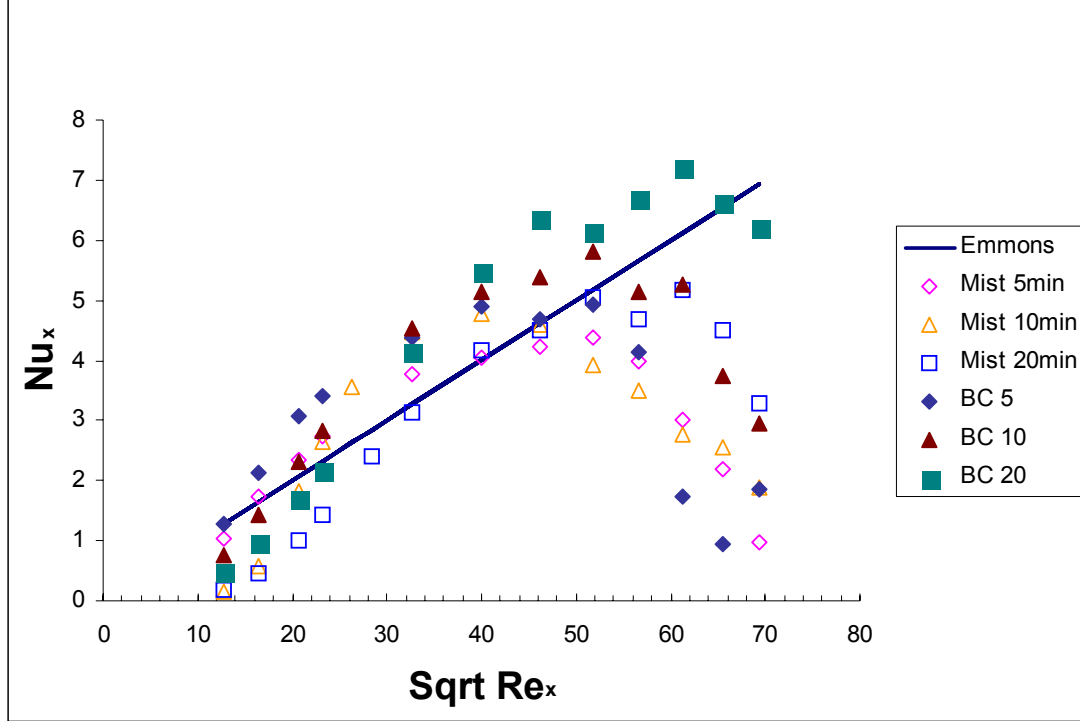


Figure 5: Normalized Burning Rate Nu_x versus $Re_x^{0.5}$ in 5, 10 and 20-minute tests with 4.3% NanoMist and Base case $U_\infty = 84$ cm/s

Since the heat feedback rate to the surface in this section is much less in the NanoMist test compared to the base case, the PMMA plate would take longer time to warm up and start pyrolyzing vigorously. Therefore steady state is attained later in the mist case than in the base case. For example in 20 minutes the base case seem to be approaching steady state downstream up to about $Re_x^{0.5} \sim 60$ ($X=70$ mm). On the other hand, in the mist case, burning rate seems to be approaching steady state in 20 minutes only up to $Re_x^{0.5} \sim 50$ ($X= 50$ mm).

Next we present the effects of mist from spray nozzles on the burning rate of the PMMA plate. Figure 6 is a plot of Nu_x versus $Re_x^{0.5}$ in tests with one of the spray nozzles, SC3. Figure 6 shows results in 5, 10, 15 and 20-minute tests with and without mist. All the tests were conducted with U_∞ of 84 cm/s. For small $Re_x^{0.5}$ the burning rate is suppressed by mist addition mainly by the establishment of a quench zone near the upstream edge. In this region the base case data show the curvature driven transient burning rate but the mist data do not. This is attributed to the effects of presence of a quench zone in this region. The timed tests were conducted independently and the exact length of the quench distance cannot be duplicated each time. Thus the Nu_x at various burn-times were not consistent with respect to time.

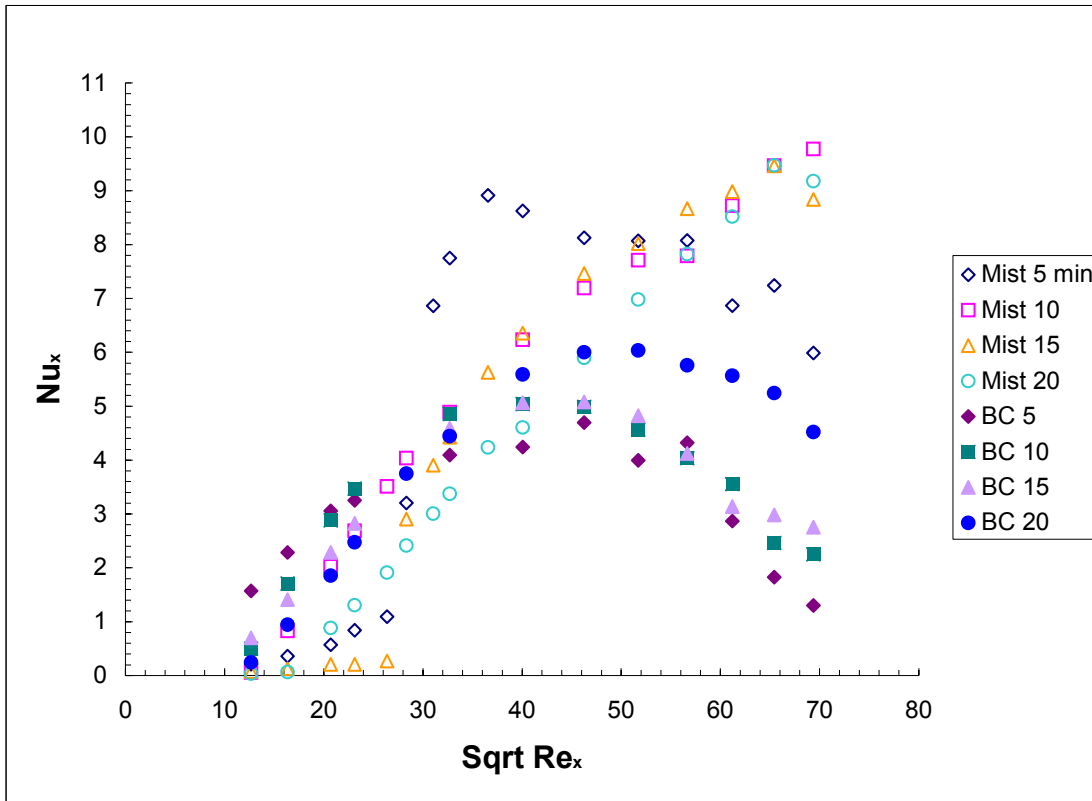


Figure 6: Normalized Burning Rate Nu_x versus $Re_x^{0.5}$ in 5, 10, 15 and 20-minute tests with SC3 and Base case $U_\infty = 84$ cm/s

For large $Re_x^{0.5}$ (downstream), the data show that for each test duration the local burning rates are significantly higher with mist than without mist. For example for $Re_x^{0.5} \sim 50$, the Nu_x in 5, 10 and 20-minute base case tests are about 4, 4.5 and 6, respectively; while the corresponding numbers for the SC3 mist tests are about 8, 7.7 and 7 respectively. This is consistent with the temperature results, which clearly shows that the heat feedback rate to the surface downstream increases when spray nozzle mist was added (Fig.4). For $30 < Re_x^{0.5} < 50$ the 5-minute mist data in Fig. 6 show very high burning rates (higher than the other times). This is the effect of the quench zone. The leading edge of the flame is anchored within this region during the 5 minutes and since the heat feedback is very high in this region within this time, the burning rate is very high. Recall that the flame slowly spreads upstream with time.

In the base case tests the local burning rate in the downstream section is still increasing up to 20 minute after ignition. However, with mist the burning rate seems to have reached steady state between 10 and 20 minutes for $Re_x^{0.5} > 30$. This is clearly shown in the Fig. 6, where the data points cluster around a straight line in this section. Recall that Emmons's steady state prediction and Ananth's [3] steady state numerical solution show a linear relationship. Thus, with pressure atomizing nozzles, the downstream burning rate attains steady state faster than without mist. This is due to the increased heat feedback rate as was revealed by the temperature profiles in Fig. 4.

Figures 2 and 4 show that the spray of mist into the wind tunnel induced turbulence, which is highly manifested in the downstream section. Mist-induced turbulence is related to the incoming droplet momentum density at the point of spray injection M . M can be estimated as

$$M = N_d d_d^3 \rho_w Q / (6 d_o^2), \quad (3)$$

where N_d , d_d , ρ_w , Q , and d_o are droplet number density, droplet volume mean diameter, density of water, nozzle flow rate at the test pressure and nozzle orifice diameter, respectively. The droplet number density and mean volume diameter are obtained from data measured with Malvern Spraytec[®] at the exit of the tunnel, which are approximations of the values at the exit of the nozzles. For the 4 nozzles SC1, SC2, SC3 and SC4 the estimated M are 3.21, 3.29, 2.61 and 2.46 g/cm²s, respectively.

The data presented in Figs 4 and 6, strongly suggest that the effects of flame fluctuations led to increased heat feedback to the PMMA surface and therefore increased burning rate. To verify this we present a plot of Nu_x versus dimensionless temperature variation θ , where $\theta = T_\sigma / T_{ave}$. T_σ and T_{ave} are the temperature standard deviation and average temperature of each set of 100 temperature data measured at various locations (Fig.2). Figure 7 shows Nu_x versus θ for measurements at one point upstream ($X = 22$ mm $Y = 4$ mm) and two points downstream ($X = 57$ mm $Y = 8$ mm and $X = 78$ mm $Y = 12$ mm). All the points are on the air side of the diffusion flame where instabilities are greater [13]. The estimated droplet momentum density M for each test is written against the datum on Fig.7. In this way the spray disturbance can be related to the temperature fluctuation and to the burning rate. For the base case there is no induced turbulence and $M = 0.0$. In the leading section Nu_x does not correlate with θ or with M . Indeed the difference between the base case and the mist cases are insignificant. However, downstream Nu_x correlates with both θ and M . As momentum density increases, flame fluctuation (turbulence) increases and burning rate increases. For example at $X = 57$ mm, $Y = 8$ mm Nu_x increases between ~ 4 and ~ 10 as θ increases between ~ 0.01 and 0.16 and M increases between 0.0 and 3.21 g/cm²s. Similarly at $X = 78$ mm $Y = 12$ mm; Nu_x increases between ~ 1.6 and ~ 12 as θ increases between ~ 0.04 and 0.18 and M increases between 0.0 and 3.21 g/cm²s. Thus the effects of turbulence increases with X and so does burning rate enhancement. This is shown clearly in Fig. 7 and also in Fig.8.

Figure 8 summarizes the result of the tests with NanoMist and pressure atomizing spray nozzles. It shows a plot the normalized change in burning rate at each X location versus $Re_x^{0.5}$. The normalized change is obtained as the difference between the burning rate with and without mist divided by the base case burning rate. The negative data represent suppression, while the positive data represent enhancement. The droplet momentum densities estimated for spray nozzle mist are 3.21, 3.29, 2.61, and 2.46 g/cm²s for SC1, SC2, SC3 and SC4, respectively. Figure 8 shows that burning rate was suppressed in tests

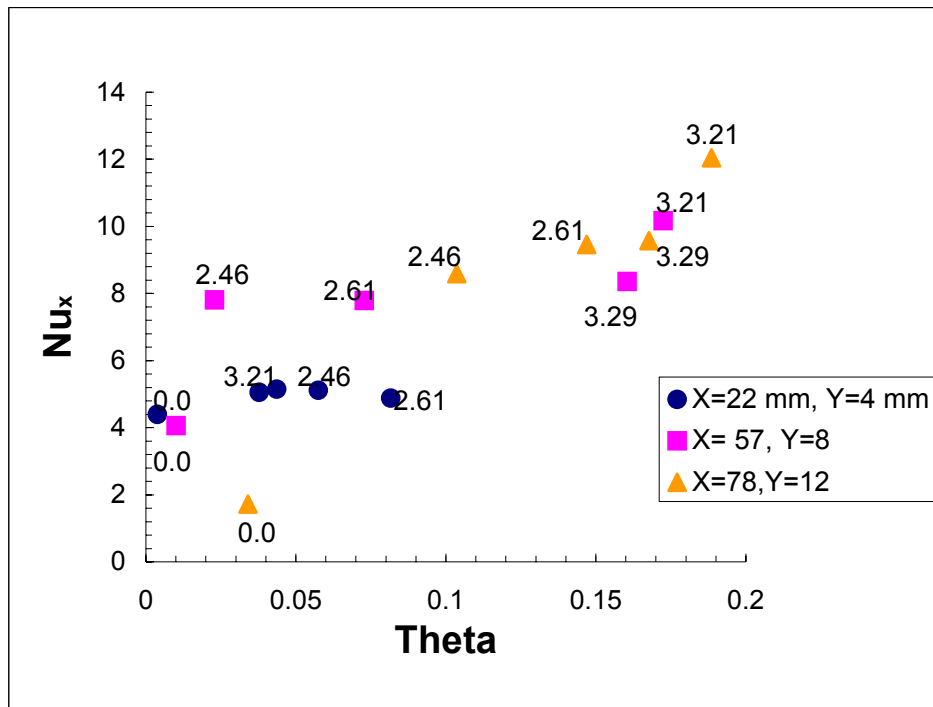


Figure 7: Variation of burning rate Nu_x with dimensionless temperature fluctuation θ at various locations in the flame

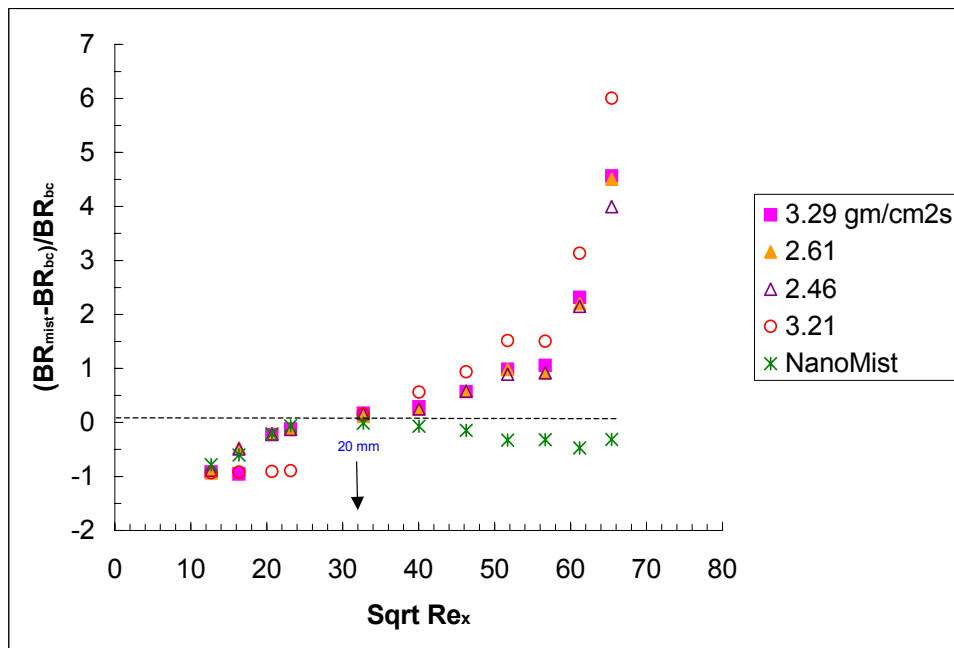


Figure 8: Change in burning rate as a result of mist in 10-minute tests with NanoMist and pressure atomizing nozzles $U_\infty = 84$ cm/s

with spray nozzles and NanoMist for $Re_x^{0.5} < 32$, which corresponds to the leading 20 mm of the plate. In this section, burning rate was suppressed by as much as 80%. However for $Re_x^{0.5} > 32$ ($X > 20$ mm) the burning rate was enhanced in tests with all the nozzles but it was suppressed in the NanoMist tests. With NanoMist burning rate was suppressed downstream by as much as 30%. However, with SC1 at high induced a momentum ($3.21 \text{ g/cm}^2\text{s}$), the burning rate was enhanced by as much as 6 times near the PMMA trailing edge. It is also interesting to note in Fig. 8 that burning rate enhancement increased sharply for $Re_x^{0.5} > 50$. Burning rate is enhanced by about 100% between $30 < Re_x^{0.5} < 52$ ($20 < X < 60$ mm) but it is enhanced by about 5 times between $52 < Re_x^{0.5} < 65$ ($60 < X < 80$ mm). Thus Fig.8 further confirms the strong correlation between the spray-induced turbulence and the enhanced local burning rate in mist tests in the trailing section.

4.0 CONCLUSIONS

In the preceding section results of experiments to investigate the effects of air-borne water mist on the forced convection boundary layer combustion of PMMA plates were presented. Fine water droplets with $SMD < 50 \mu\text{m}$ were injected into the incoming airflow at $U_\infty = 84 \text{ cm/s}$. Mist with $10 \mu\text{m} < SMD < 50 \mu\text{m}$ was sprayed co-currently into the wind tunnel from pressure atomizing nozzles. NanoMist with $SMD \sim 3 \mu\text{m}$ was introduced from an ultrasonic mist generator. The time-averaged local burning rates were measured and gas phase temperature profiles were mapped in tests with and without water mist. Analysis of the results reveals the following:

- In the PMMA leading section, the burning rate is suppressed by both NanoMist and spray nozzle mist. However, the larger droplets seem to evaporate closer to the flame front than NanoMist droplets. Thus more effective use of latent heat is made with the larger droplets and therefore a lower concentration of the larger droplets is required to extinguish the flame.
- In the trailing section of the plate, the effects of water mist are opposite in the two systems. The introduction of mist from spray nozzles enhanced the burning rate instead of suppressing it. It seems that the effects of mist-induced turbulence helped increase the heat feedback rate to the surface and therefore the burning rate. The data show a correlation between the injection momentum density of droplets, the fluctuation in flame temperature in the trailing section and the enhanced plate regression rate in this section. On the other hand, with NanoMist, where induced turbulence is minimal the cooling effects reduces the heat feedback rate and hence the burning rate is suppressed. Furthermore, steady state burning rate is approached faster in this section in the tests with nozzles, where the heat feedback rate is higher than in the base case. However, with NanoMist, where the heat feedback rate is less than in the base case the transient takes longer time to approach steady state.

5.0 ACKNOWLEDGEMENTS

We appreciate the contributions of Dr. Patricia Tatem Mr. Daniel MacArthur and Mr. Clarence Whitehurst in this work. This work was funded by the office of Naval Research, through Naval Research Laboratory and Code 334, under the Damage Control Task of the FY03 Surface Ship Hull, Mechanical and Electrical Technology Program

6. REFERENCES

1. Tamanini, F. A study of the extinguishments of vertical wood slabs in self-sustained burning by water spray application” *Combust. Sci. and Tech* **14**: 1-15 (1976)
2. Magee, R.S and Reitz, R.D “Extinguishment of radiation augmented plastic fires by water mist” *Proc Combust. Inst.* **15**: 337-347 (1975)
3. Ananth R ; Ndubizu C C and Tatem P.A “Burning rate distributions for boundary layer flow combustion of a PMMA plate in forced flow” *Combustion and Flame* **135** (2003) pp 35-55.
4. Ndubizu, C.C; Ananth,R.; Tatem, P.A “Transient burning rate of a Non-charring plate under a forced flow boundary layer flame” Paper submitted for publication in *Combustion and Flame*.
5. Zhuo L and Fernandez-Pello A.C “Turbulent burning of a flat fuel surface” *Fire Safety Science: Proceedings of the third International Symposium*, Hemisphere. Washington D.C pp. 414-424 (1990)
6. Ahmad T and Faeth G.M “Turbulent wall fires “ *Proc. Combust Inst.* **17** pp1149 (1978)
7. Ndubizu C; Ananth R; Williams F.W “Water mist Suppression of PMMA boundary layer combustion - A Comparison of NanoMist and Spray nozzle performance.” Naval Research Laboratory Memorandum report NRL/MR/6180-04- (2004)
8. Ndubizu, C.C; Ananth,R.; Tatem, P.A; and Motevalli, V; “On Water mist fire suppression mechanisms in a gaseous diffusion flame” *Fires Safety J.* **31:3** p.253 (1998)
9. Ndubizu C C Ananth R and Tatem P.A “The burning of a thermoplastic material under a forced-flow boundary layer flame” Naval Research Laboratory Memorandum report NRL/MR/6180-02-8630 (2002)
10. Ndubizu C; Ananth R; Tatem P A “ Boundary layer flame spread over PMMA within the quench zone: A moving boundary effect” *Combust. Sci. Tech.* **175:1** p.1-26 (2003)
11. Tewarson A, “Generation of heat and chemical compounds in fires” In *SFPE Handbook of Fire protection Engineering*. P.J. DiNenno et. al (Eds.). National Fire Protection Association, Quincy, MA (1995) p. 3-68.
12. R Ananth; C.C Ndubizu and P.A Tatem “Pyrolysis and boundary layer combustion of a non-charring solid plate under forced flow” Naval Research Laboratory Memorandum report NRL/MR/6180-03-8700 (2003)
13. Ahmad T and Faeth G.M “Investigation of the laminar over fire region along upright surfaces” *J. Heat Transfer* **100** (1978) 112-119